HHS Public Access

Author manuscript

Angew Chem Int Ed Engl. Author manuscript; available in PMC 2025 May 21.

Published in final edited form as:

Angew Chem Int Ed Engl. 2024 May 21; 63(21): e202402178. doi:10.1002/anie.202402178.

RNA Control via Redox-Responsive Acylation

Junsong Guo[+],
Department of Chemistry, National University of Singapore, 4 Science Drive 2, Singapore 117544, Singapore

Siqin Chen[+],
Department of Chemistry, National University of Singapore, 4 Science Drive 2, Singapore 117544, Singapore

Yoshiyuki Onishi,
Department of Chemistry, Stanford University, Stanford, CA 94305, USA

Qi Shi,
Department of Chemistry, National University of Singapore, 4 Science Drive 2, Singapore 117544, Singapore

Yangyang Song,
Cancer Science Institute of Singapore, National University of Singapore, 14 Medical Dr, Singapore 117599, Singapore

Hui Mei,
Department of Chemistry, Stanford University, Stanford, CA 94305, USA

Leilei Chen,
Cancer Science Institute of Singapore, National University of Singapore, 14 Medical Dr, Singapore 117599, Singapore

Eric T. Kool[*],
Department of Chemistry, Stanford University, Stanford, CA 94305, USA

Ru-Yi Zhu[*]
Department of Chemistry, National University of Singapore, 4 Science Drive 2, Singapore 117544, Singapore

Abstract

Incorporating stimuli-responsive components into RNA constructs provides precise spatiotemporal control over RNA structures and functions. Despite considerable advancements, the utilization of redox-responsive stimuli for the activation of caged RNAs remains scarce. In this context, we present a novel strategy that leverages post-synthetic acylation coupled with redox-responsive

[*] rzhu@nus.edu.sg, kool@stanford.edu.
[+]These authors contribute equally to this work.

Conflict of Interest
The authors declare no conflict of interest.

chemistry to exert control over RNA. To achieve this, we design and synthesize a series of acylating reagents specifically tailored for introducing disulfide-containing acyl adducts into the 2′-OH groups of RNA (“cloaking”). Our data reveal that these acyl moieties can be readily appended, effectively blocking RNA catalytic activity and folding. We also demonstrate the traceless release and reactivation of caged RNAs (“uncloaking”) through reducing stimuli. By employing this strategy, RNA exhibits rapid cellular uptake, effective distribution and activation in the cytosol without lysosomal entrapment. We anticipate that our methodology will be accessible to laboratories engaged in RNA biology and holds promise as a versatile platform for RNA-based applications.

Keywords

Post-synthetic acylation; Reducing environment; RNA; Disulfide; Cloaking

Introduction

RNA molecules exhibit remarkable versatility and encapsulate extensive biological information,[1] endowing the biomolecules with multiple functions including protein synthesis,[1a] gene regulation,[2] catalysis,[3] and signal transduction.[4] This multifaceted biology has fueled the exploration of RNA’s utility in diverse fields.[5] In line with the sophisticated mechanisms employed by nature to temporally and spatially govern various aspects of RNA biogenesis,[6] achieving precise control over RNAs has become an important goal.[7] This imperative arises from the necessity to comprehensively investigate the functional intricacies of RNAs and effectively harness their applications.[8]

Several methods have been investigated to establish stimulus-responsive RNA, allowing for the precise modulation of its structures and functions. In the early stage, trichloroethyl moieties were incorporated into constructs through solid-phase synthesis for chemical control over RNA.[9] Advances in photoreversible blocking strategies have further facilitated spatiotemporal manipulation of RNAs.[10] Photocaging groups integrated into oligonucleotides can be selectively removed upon photoirradiation. Although efficacious, most of methods heavily rely on solid-phase synthesis, involving customized phosphoramidites, rendering it inaccessible to non-specialized laboratories and, significantly, confined to short oligonucleotides. To address these limitations, the post-synthetic acylation of 2′-OH groups of RNA utilizing acylimidazole reagents has emerged as a useful strategy for functionalization of RNA, irrespective of its origin or length.[8b] The structure and function of acylated RNA can be restored through either phosphine-triggered Staudinger reduction[11] or UV light irradiation.[12] Nevertheless, a significant issue is the toxicity of high concentrations of phosphine and UV light exposure in cell-based experiments.[13] More recently, the Heemstra group employed glyoxal to thermoreversibly control various nucleic acid scaffolds.[7c] While glyoxalation offers a versatile strategy for RNA caging, the inherent thermal instability necessitates the protection of nucleic acids from heat during manufacturing, storage and utilization.

Despite these encouraging advancements, redox-responsive control RNA is still highly unexplored, and a prevalent constraint in current methodologies is the need for transfection reagents to transport RNA into the cytosol in cell-based experiments. Notably, Abe and co-workers demonstrated that the incorporation of repeat disulfide units at the terminus of nucleic acids facilitated the cytosolic internalization of oligonucleotides through disulfide exchange reactions with thiols present on the cell surface.[14] The Lu group further reported the delivery of aptamers into plant cells for biosensing by introducing a disulfide-modified helper strand.[15] Additionally, prodrug-type synthetic oligonucleotides can also penetrate the cell membrane and be activated within the reductive cytosolic milieu.[16] These findings highlight the effective role of disulfides in promoting the cellular distribution of nucleic acids. Both the internalization and activation of oligonucleotides depend on the reducing cellular environment.

Inspired by these studies, we conceived a redox-responsive strategy to modulate RNA structures and functions by incorporating disulfide units via post-synthetic RNA acylation. RNA modified with multiple disulfide units had the potential to cross the cell membrane through thiol-disulfide exchange reactions,[14a,17] obviating the need for transfection reagents. The disulfide-containing RNA can potentially be restored by external reducing stimuli in vitro or the reducing intracellular environment. In comparison with technically challenging and labor-intensive solid-phase oligonucleotide synthesis, post-synthetic acylation of RNA could provide a simple and general strategy for appending functional groups on existing RNAs. To this end, we design and synthesize a series of acylating reagents (ARs) as illustrated in Figure 1a. These ARs can acylate 2′-OH groups of RNA, with multiple acyl adducts installed per strand (“cloaking”). The introduced disulfide-containing acyl groups effectively block RNA catalytic activity, small-molecule binding and folding, while enhancing the cellular uptake of cloaked RNAs. We further demonstrate that the reducing environment can trigger the reduction of disulfide bonds, resulting in the intramolecular cyclization of the reduced intermediate and the subsequent liberation and activation of cloaked RNAs (“uncloaking”).

Results and Discussion

To achieve this redox-responsive RNA acylation, we investigated the impact of AR structures on RNA cloaking, uncloaking, and cellular uptake. The ARs were composed of three distinct functional components (Figure 1a): (1) an electrophilic acylation group, acyl imidazole,[18] designed for conjugating with 2′-OH groups of RNA; (2) an exchange warhead, *tert*-butyl thiol or 2-mercaptopyridine, employed to mediate the cellular uptake; and (3) a redox-responsive self-immolative linker capable of forming a thermodynamically stable five- or six-membered ring. To refine the self-immolative property, four alkyl chains with variations in length and substitution were selected.

We then chose a FAM-labeled 18-nucleotide (nt) RNA (^{FAM}RNA) as a model for cloaking analysis. RNA cloaking was conducted by mixing ^{FAM}RNA with AR in a DMSO/H_2O solvent system at room temperature for 4 h, followed by purification of the resultant RNA through ethanol precipitation. We prepared a panel of ^{FAM}RNAs with different acyl substituents, denoted as ^{FAM}RNA-**1**-**8**. The acylation levels were characterized using

MALDI-TOF mass spectrometry (MS), as depicted in Figure 1b. Notably, ARs **5** and **6** displayed high levels of acylation, with a median modification of 4.5 added acyl groups per strand (out of 18-nt), while ARs **1**, **4**, and **7** showed a slightly lower degree of acylation. In contrast, ARs **2** and **3** gave minimal acyl labels in ^{FAM}RNA even with extended reaction time and higher concentrations (Figure S1); limited solubility may account for the poor acylation ability as ARs **2** and **3** have more carbon atoms than ARs **1** and **4**. Surprisingly, AR **8** was found to be poorly soluble and as a result inferior acylation reactivity was observed. We also demonstrated that the most reactive ARs **5** and **6** showed concentration-dependent acylation, as analyzed by denaturing PAGE and MALDI-TOF MS (Figures S2 and S3). To examine the selectivity of AR towards 2′-OH groups, we treated ^{FAM}DNA, the DNA version of ^{FAM}RNA, with ARs **5** and **6**, and found substantially lower reactivity and a limited number of adducts (Figures S4a and S5). These results suggest primary reaction at 2′-OH groups of ^{FAM}RNA, with low background levels of acylation at the FAM label, hydroxyl groups at RMA/DNA termini, and/or nucleobases, consistent with previous studies.[11a,12a,19] Notably, negligible acylation on DNA fully modified with phosphorothioate (PS) groups was observed, clearly indicating ineffective reaction between PS groups and AR **5** or **6** (Figure S4b).

Subsequently, we examined whether the cloaked RNA could be restored in a reducing environment. Uncloaking kinetics experiments were carried out on cloaked ^{FAM}RNAs in the presence of 10 mM dithiothreitol (DTT) at 37°C (Figure 2a). The resulting RNAs were initially analyzed by denaturing PAGE. Upon incubation of ^{FAM}RNA-**5** or ^{FAM}RNA-**6** with DTT, a time-dependent uncloaking of RNA was observed (Figures 2b and S6). Within 4 h, uncloaking of ^{FAM} RNA-**5** was nearly complete. By contrast, ^{FAM}RNA-**6** exhibited lower sensitivity to DTT treatment, achieving full restoration within 60 h, presumably due to the slower intramolecular cyclization kinetics of the self-immolative linker in the reduced intermediate. Notably, biologically more relevant glutathione (GSH) was shown to restore the cloaked RNA with similar efficiency to DTT (Figure S7). We also quantitively monitored the uncloaking process of cloaked ^{FAM}RNA with MALDI-TOF MS. Exposure to DTT resulted in a rapid reduction of disulfide bonds in ^{FAM}RNA-**5** (Figure 2c), with no detectable disulfides remaining within only 30 min of incubation, and RNA recovery was detected within 30 min as well. The rate-limiting step of ^{FAM}RNA-**5** release is likely the intramolecular cyclization as complete removal of reduced acyl groups requires prolonged incubation (6 h). In accordance with our proposed self-immolation mechanism, 4-butyrothiolactone, the byproduct after uncloaking, was detected by GC-MS (Figures 2a and S8). Similarly, ^{FAM}RNA-**6** underwent rapid disulfide reduction followed by relatively slow intramolecular cyclization to fully restore RNA within 60 h (Figure S9), aligning well with the result from denaturing PAGE (Figure S6).

Next, we proceeded to explore the utilization of AR **5** in controlling the catalytic activity of RNA (Figure 3a). The 10–23 ribozyme was chosen due to its capacity to hybridize with a single-stranded substrate RNA and form a tertiary structure in the presence of magnesium ions, ultimately leading to cleavage of the substrate RNA.[10f,20] The ribozyme was modified with AR **5** using the established acylation method, and the acylation level was characterized by MALDI-TOF MS (Figure S10). We subsequently evaluated the catalytic activity of

cloaked ribozyme against the substrate, observing abolished activity in RNA cleavage (Figure 3b). In contrast, the unmodified ribozyme converted most of the substrate in 1.5 h. Importantly, this catalytic inactivation was reversible upon the removal of introduced acyl adducts. Treatment of the cloaked ribozyme with DTT (10 mM) resulted in substrate cleavage comparable to that achieved by the unmodified ribozyme. Further examining the cleavage kinetics, we found that the cloaked ribozyme exhibited no detectable activity towards the substrate at different time points (Figure S11), while the high conversion efficiency of the uncloaked ribozyme mirrored that of the untreated one (Figure 3c,3d). These data underscore the efficacy of our approach in controlling RNA catalysis.

The above experiments were focused on short synthetic RNAs. While biologically relevant RNAs often encompass longer sequences, it is challenging to incorporate functional groups into constructs through solid-phase synthesis. To demonstrate the feasibility of controlling long RNA by this acylation strategy, we opted for the Pepper aptamer, a recently reported fluorogenic RNA designed for imaging (Figure 4a).[21] This RNA aptamer, consisting of approximately 100 nt, assumes a compact three-dimensional structure, resulting in green fluorescence after the binding of the HBC dye. The Pepper aptamer was in vitro transcribed and purified, followed by cloaking with AR **5**. The untreated and cloaked Pepper aptamer samples were then respectively dissolved in a folding buffer, and the HBC dye was introduced. Intriguingly, the cloaked Pepper aptamer exhibited a complete loss of fluorescence, while the untreated counterpart displayed robust fluorescence emission (Figures 4b and S12). Conversely, DTT treatment resulted in the fluorescence signal of the cloaked Pepper aptamer comparable to that of the untreated one. Next, we explored the uncloaking kinetics of the cloaked Pepper aptamer by incubation with DTT for different durations (Figures 4c,4d, and S13). A rapid augmentation in the fluorescence signal of Pepper aptamer was discerned within 2 h. The cloaked Pepper aptamer restored its original fluorogenic state after 6-h DTT incubation. Collectively, these results validate that the cloaking suffices to disrupt the binding of HBC dye to RNA aptamer, and the removal of acyl adducts reinstates the fluorogenic activity of the Pepper aptamer, affirming the adaptability of our acylation strategy to RNAs of greater length than those typically synthesized using solid-phase synthesis.

Another objective of our research was to employ ARs for transporting RNA into cells. To validate this, the cellular uptake of ^{FAM}RNA-**1**-**8** was systematically evaluated in HeLa cells through confocal laser scanning microscopy (CLSM). In brief, cloaked or unmodified ^{FAM}RNA (200 nM) was administered to cells for 1 h at 37°C before imaging. The well-distributed green fluorescence signals were observed in cells treated with ^{FAM}RNA-**5** and ^{FAM}RNA-**6** (Figure 5a,5b), whereas ^{FAM}RNA-**7** and ^{FAM}RNA-**8** exhibited relatively less pronounced fluorescent signals. These results reveal a positive correlation between the degree of acylation (Figure 1b) and the cellular uptake of RNA. However, fluorescence signals of cells incubated with ^{FAM}RNA-**1**-**4** were minimal, indicative of the limited enhancement in RNA cell permeability, possibly due to the relatively lower acylation levels or reaction activity during thiol-disulfide exchange. As anticipated, negligible green fluorescence was detected in cells incubated with unmodified ^{FAM}RNA, suggesting that cloaked RNAs have better access to cells, in contrast with unmodified RNA. Quantitative

assessment of the cellular internalization of ^{FAM}RNA-**1**–**8** was subsequently conducted through flow cytometry analysis (Figure 5c,5d). After a 1-h incubation, ^{FAM}RNA-**5**–**7** manifested stronger fluorescence signals in cells than ^{FAM}RNA-**1**–**4** and **8**. These results align with the observations from CLSM images, supporting that disulfide-containing acyl adducts facilitate the cellular internalization of RNA.

Small interfering RNA (siRNA) has garnered significant attention in the field of gene therapy,[22] yet there remains an ongoing need for efficacious methods to enhance its intracellular applications.[23] We contemplated the potential applicability of the cloaking strategy to siRNA. To this end, siRNA targeting green fluorescent protein (siGFP) was employed as a model. Building upon the results gained from cellular uptake studies, disulfide-containing acyl adducts were introduced into siGFP using AR **5** (siGFP-**5**), and the acylation level was characterized by MALDI-TOF MS (Figure S14). The RNA interference (RNAi) efficacy of siGFP-**5** was assessed in HEK293T cells that stably express GFP. After incubation with siGFP-**5**, the cells were visualized using CLSM (Figure 5e,5f). The fluorescence intensity of cells incubated with siGFP-**5** was lower than that of untreated cells or cells incubated with unmodified siGFP, implying not only the successful internalization of siGFP-**5** into the cytosol but also activation by the intracellular reducing environment. The downregulation of GFP expression provides evidence that the incorporation of disulfide-containing acyl moieties enhances the cellular uptake of RNA, and this control strategy is compatible with the intracellular reducing environment.

To elucidate the intracellular localization and uptake kinetics of cloaked RNA (with ^{FAM}RNA-**5** as a representative), we conducted a time-course live-cell imaging in HeLa cells co-stained with Hoechst nuclear stain and lysosomal tracker. As illustrated in Figure 6a, the green fluorescence of ^{FAM}RNA-**5** began to accumulate around the cell membrane within 5 min of incubation. Within 10 min, the fluorescence signals exhibited a substantial increase on the cell surface, potentially attributable to the formation of covalent disulfide bonds between cloaked RNA and exofacial thiols. Extending the incubation time to 20 min facilitated the significant transfer of ^{FAM}RNA-**5** to the cytosol. The green fluorescence remained stably distributed in the cytosol until cells were exposed to ^{FAM}RNA-**5** for 30 min. Notably, despite prolonged incubation, the green fluorescence signals from ^{FAM}RNA-**5** did not co-localize with the red fluorescent lysosomes, indicating the absence of lysosomal entrapment throughout the process (Figure 6b). These results reveal the rapid and effective distribution of cloaked RNA within the cytosol. To investigate whether the cellular internalization of cloaked RNA occurs through the formation of disulfide bonds on the cell surface, cells were pre-treated with 5,5’-dithiobis-(2-nitrobenzoic acid) (DTNB) or sodium iodoacetate (SI) to block free thiols on the cell membrane before ^{FAM}RNA-**5** incubation.[24] The CLSM results (Figure S15) showed a reduction in fluorescence signals in the presence of Supporting Information (decreased by approximately 64%) or DTNB (decreased by approximately 73%), in contrast with cells treated solely with ^{FAM}RNA-**5**. Importantly, no nanostructures via supramolecular assembly before or after RNA cloaking was observed by dynamic light scattering experiments (Figure S16 and Table S1), ruling out the possibility of RNA uptake through the formation of nanoparticles. These results were consistent with previous reports,[14a,15] indicating the essential role of thiol-disulfide exchange reactions

with cell surface thiols in the cellular uptake of cloaked RNA, while acknowledging the need for further investigations into the precise internalization mechanisms.

Conclusion

We have devised a redox-responsive strategy for control of RNAs through a single post-synthetic cloaking step. A set of ARs was employed to covalently incorporate disulfide-containing moieties into RNA sequences via 2′-OH acylation, displaying notable acylation efficiency. These introduced acyl adducts exert potent disruptive effects on RNA catalytic activity and folding, effectively inhibiting ribozyme-mediated cleavage activity and small molecule binding to RNA aptamer. Importantly, treatment with the reducing stimuli initiates the reduction of disulfide bonds, leading to the spontaneous removal of acyl groups and subsequent activation of ribozyme and aptamer. Our data also demonstrate that RNAs with disulfide-containing acyl moieties can be efficiently internalized into cells, presumably benefiting from disulfide exchange with thiols on the cell membrane. Moreover, we show that cloaked siGFP can effectively suppress gene expression of GFP in living mammalian cells. Time-lapse imaging of cloaked RNA uptake indicates a rapid cellular internalization mode without lysosomal trapping. These findings underscore the compatibility of our redox-responsive control approach both in vitro and in cellular reducing environments, affirming its great potential for RNA-based applications.

Supplementary Material

Refer to Web version on PubMed Central for supplementary material.

Acknowledgements

This research was supported by the National University of Singapore Presidential Young Professorship start-up grant (A-0008363-00-00 to R.Y.Z) and white space funding (A-0008363-01-00 to R.Y.Z). We are grateful to Prof. Anh Tuân Phan and his team at Nanyang Technological University for MALDI-TOF analysis. E.T.K. acknowledges support from the U.S. National Institutes of Health (GM127295, GM145357) and Y.O. acknowledges Daiichi Sankyo Corporation for support of a Visiting Scientist position. L.C. acknowledges support from the Health and Biomedical Sciences Industry Alignment Fund Pre-Positioning (IAF-PP, H20C6a0034).

Data Availability Statement

The data that support the findings of this study are available in the supplementary material of this article.

References

[1]. a)Cech TR, Steitz JA, Cell 2014, 157, 77–94; [PubMed: 24679528] b)Armitage BA, Curr. Opin. Chem. Biol. 2011, 15, 806–812; [PubMed: 22055496] c)Lieberman J, Nat. Struct. Mol. Biol. 2018, 25, 357–364. [PubMed: 29662218]

[2]. Anastasiadou E, Jacob LS, Slack FJ, Nat. Rev. Cancer 2018, 18, 5–18. [PubMed: 29170536]

[3]. a)Doherty EA, Doudna JA, Annu. Rev. Biochem. 2000, 69, 597–615; [PubMed: 10966470] b)Serganov A, Patel DJ, Nat. Rev. Genet. 2007, 8, 776–790. [PubMed: 17846637]

[4]. Lin C, Yang L, Trends Cell Biol. 2018, 28, 287–301. [PubMed: 29274663]

[5]. a)Jasinski D, Haque F, Binzel DW, Guo P, ACS Nano 2017, 11, 1142–1164; [PubMed: 28045501] b)Sullenger BA, Nair S, Science 2016, 352, 1417–1420; [PubMed: 27313039] c)Isaacs FJ,

Dwyer DJ, Collins JJ, Nat. Biotechnol. 2006, 24, 545–554; [PubMed: 16680139] d)Dunn MR, Jimenez RM, Chaput JC, Nat. Chem. Rev. 2017, 1, 0076;e)Serganov A, Nudler E, Cell 2013, 152, 17–24. [PubMed: 23332744]

[6]. a)Chen LL, Nat. Rev. Mol. Cell Biol. 2016, 17, 205–211; [PubMed: 26908011] b)Roundtree IA, Evans ME, Pan T, He C, Cell 2017, 169, 1187–1200. [PubMed: 28622506]

[7]. a)Lubbe AS, Szymanski W, Feringa BL, Chem. Soc. Rev. 2017, 46, 1052–1079; [PubMed: 28128377] b)Brieke C, Rohrbach F, Gottschalk A, Mayer G, Heckel A, Angew. Chem. Int. Ed. 2012, 51, 8446–8476;c)Knutson SD, Sanford AA, Swenson CS, Korn MM, Manuel BA, Heemstra JM, J. Am. Chem. Soc. 2020, 142, 17766–17781; [PubMed: 33017148] d)Kushwaha M, Rostain W, Prakash S, Duncan JN, Jaramillo A, ACS Synth. Biol. 2016, 5, 795–809. [PubMed: 26999422]

[8]. a)Li F, Dong J, Hu X, Gong W, Li J, Shen J, Tian H, Wang J, Angew. Chem. Int. Ed. 2015, 54, 4597–4602;b)Velema WA, Kool ET, Nat. Chem. Rev. 2020, 4, 22–37.

[9]. Höbartner C, Mittendorfer H, Breuker K, Micura R, Angew. Chem. Int. Ed. 2004, 43, 3922–3925.

[10]. a)Govan JM, Young DD, Lusic H, Liu Q, Lively MO, Deiters A, Nucleic Acids Res. 2013, 41, 10518–10528; [PubMed: 24021631] b)Ando H, Furuta T, Tsien RY, Okamoto H, Nat. Genet. 2001, 28, 317–325; [PubMed: 11479592] c)Wu L, Wang Y, Wu J, Lv C, Wang J, Tang X, Nucleic Acids Res. 2013, 41, 677–686; [PubMed: 23104375] d)Lucas T, Schäfer F, Müller P, Eming SA, Heckel A, Dimmeler S, Nat. Commun. 2017, 8, 15162; [PubMed: 28462946] e)Chaulk SG, MacMillan AM, Nat. Protoc. 2007, 2, 1052–1058; [PubMed: 17546010] f)Chaulk SG, MacMillan AM, Nucleic Acids Res. 1998, 26, 3173–3178; [PubMed: 9628915] g)Mikat V, Heckel A, RNA 2007, 13, 2341–2347; [PubMed: 17951332] h)Deiters A, Curr. Opin. Chem. Biol. 2009, 13, 678–686; [PubMed: 19857985] i)Meyer A, Mokhir A, Angew. Chem. Int. Ed. 2014, 53, 12840–12843;j)Lu J, Koo SC, Li NS, Piccirilli JA, Nucleosides Nucleotides Nucleic Acids 2015, 34, 114–129; [PubMed: 25621705] k)Gu C, Xiao L, Shang J, Xu X, He L, Xiang Y, Chem. Sci. 2021, 12, 9934–9945; [PubMed: 34377390] l)Höbartner C, Silverman SK, Angew. Chem. Int. Ed. 2005, 44, 7305–7309.

[11]. a)Kadina A, Kietrys AM, Kool ET, Angew. Chem. Int. Ed. 2018, 57, 3059–3063;b)Wang SR, Wu LY, Huang HY, Xiong W, Liu J, Wei L, Yin P, Tian T, Zhou X, Nat. Commun. 2020, 11, 91; [PubMed: 31900392] c)Habibian M, McKinlay C, Blake TR, Kietrys AM, Waymouth RM, Wender PA, Kool ET, Chem. Sci. 2019, 11, 1011–1016. [PubMed: 34084356]

[12]. a)Velema WA, Kietrys AM, Kool ET, J. Am. Chem. Soc. 2018, 140, 3491–3495; [PubMed: 29474085] b)Wang S, Wei L, Wang JQ, Ji H, Xiong W, Liu J, Yin P, Tian T, Zhou X, ACS Chem. Biol. 2020, 15, 1455–1463. [PubMed: 32378871]

[13]. a)Clydesdale GJ, Dandie GW, Muller HK, Immunol. Cell Biol. 2001, 79, 547–568; [PubMed: 11903614] b)McMillan TJ, Leatherman E, Ridley A, Shorrocks J, Tobi SE, Whiteside JR, J. Pharm. Pharmacol. 2008, 60, 969–976. [PubMed: 18644190]

[14]. a)Shu Z, Tanaka I, Ota A, Fushihara D, Abe N, Kawaguchi S, Nakamoto K, Tomoike F, Tada S, Ito Y, Kimura Y, Abe H, Angew. Chem. Int. Ed. 2019, 58, 6611–6615;b)Shu Z, Ota A, Takayama Y, Katsurada Y, Kusamori K, Abe N, Nakamoto K, Tomoike F, Tada S, Ito Y, Nishikawa M, Kimura Y, Abe H, Chem. Pharm. Bull. 2020, 68, 129–132;c)Hiraoka H, Shu Z, Tri Le B, Masuda K, Nakamoto K, Fangjie L, Abe N, Hashiya F, Kimura Y, Shimizu Y, Veedu RN, Abe H, ChemBioChem 2021, 22, 3437–3442. [PubMed: 34636471]

[15]. Mou Q, Xue X, Ma Y, Banik M, Garcia V, Guo W, Wang J, Song T, Chen LQ, Lu Y, Sci. Adv. 2022, 8, eabo0902. [PubMed: 35767607]

[16]. a)Ochi Y, Nakagawa O, Sakaguchi K, Wada S, Urata H, Chem. Commun. 2013, 49, 7620–7622;b)Ochi Y, Imai M, Nakagawa O, Hayashi J, Wada SI, Urata H, Bioorg. Med. Chem. Lett. 2016, 26, 845–848; [PubMed: 26755395] c)Hayashi J, Samezawa Y, Ochi Y, Wada SI, Urata H, Bioorg. Med. Chem. Lett. 2017, 27, 3135–3138; [PubMed: 28532670] d)Hayashi J, Ochi Y, Morita Y, Soubou K, Ohtomo Y, Nishigaki M, Tochiyama Y, Nakagawa O, Wada SI, Urata H, Bioorg. Med. Chem. 2018, 26, 5838–5844; [PubMed: 30420326] e)Saneyoshi H, Ohta T, Hiyoshi Y, Saneyoshi T, Ono A, Org. Lett. 2019, 21, 862–866; [PubMed: 30714380] f)Sugimoto N, Hayashi J, Funaki R, Wada SI, Wada F, Harada-Shiba M, Urata H, ChemBioChem 2023, e202300526; [PubMed: 37840006] g)Hayashi J, Nishigaki M, Ochi Y, Wada SI, Wada F, Nakagawa O, Obika S, Harada-Shiba M, Urata H, Bioorg. Med. Chem. Lett. 2018, 28, 2171–

2174; [PubMed: 29764744] h)Gauthier F, Claveau S, Bertrand JR, Vasseur JJ, Dupouy C, Debart F, Bioorg. Med. Chem. 2018, 26, 4635–4643. [PubMed: 30121212]

[17]. a)Laurent Q, Martinent R, Lim B, Pham AT, Kato T, López-Andarias J, Sakai N, Matile S, JACS Au 2021, 1, 710–728; [PubMed: 34467328] b)Yu L, Xu Y, Al-Amin M, Jiang S, Sample M, Prasad A, Stephanopoulos N, Šulc P, Yan H, J. Am. Chem. Soc. 2023, 145, 27336–27347. [PubMed: 38055928]

[18]. a)Spitale RC, Crisalli P, Flynn RA, Torre EA, Kool ET, Chang HY, Nat. Chem. Biol. 2013, 9, 18–20; [PubMed: 23178934] b)Spitale RC, Flynn RA, Zhang QC, Crisalli P, Lee B, Jung JW, Kuchelmeister HY, Batista PJ, Torre EA, Kool ET, Chang HY, Nature 2015, 519, 486–490. [PubMed: 25799993]

[19]. Habibian M, Velema WA, Kietrys AM, Onishi Y, Kool ET, Org. Lett. 2019, 21, 5413–5416. [PubMed: 31268332]

[20]. Liu Y, Wilson TJ, Lilley DMJ, Nat. Chem. Biol. 2017, 13, 508–513. [PubMed: 28263963]

[21]. a)Chen X, Zhang D, Su N, Bao B, Xie X, Zuo F, Yang L, Wang H, Jiang L, Lin Q, Fang M, Li N, Hua X, Chen Z, Bao C, Xu J, Du W, Zhang L, Zhao Y, Zhu L, Loscalzo J, Yang Y, Nat. Biotechnol. 2019, 37, 1287–1293; [PubMed: 31548726] b)Huang K, Chen X, Li C, Song Q, Li H, Zhu L, Yang Y, Ren A, Nat. Chem. Biol. 2021, 17, 1289–1295. [PubMed: 34725509]

[22]. Hu B, Zhong L, Weng Y, Peng L, Huang Y, Zhao Y, Liang XJ, Signal Transduct. Target. Ther. 2020, 5, 101. [PubMed: 32561705]

[23]. a)Juliano RL, Nucleic Acids Res. 2016, 44, 6518–6548; [PubMed: 27084936] b)Roberts TC, Langer R, Wood MJA, Nat. Rev. Drug Discovery 2020, 19, 673–694; [PubMed: 32782413] c)Zhou J, Shao Z, Liu J, Duan Q, Wang X, Li J, Yang H, ACS Appl. Bio Mater. 2020, 3, 2686–2701;d)Paunovska K, Loughrey D, Dahlman JE, Nat. Rev. Genet. 2022, 23, 265–280. [PubMed: 34983972]

[24]. Gasparini G, Sargsyan G, Bang EK, Sakai N, Matile S, Angew. Chem. Int. Ed. 2015, 54, 7328–7331.

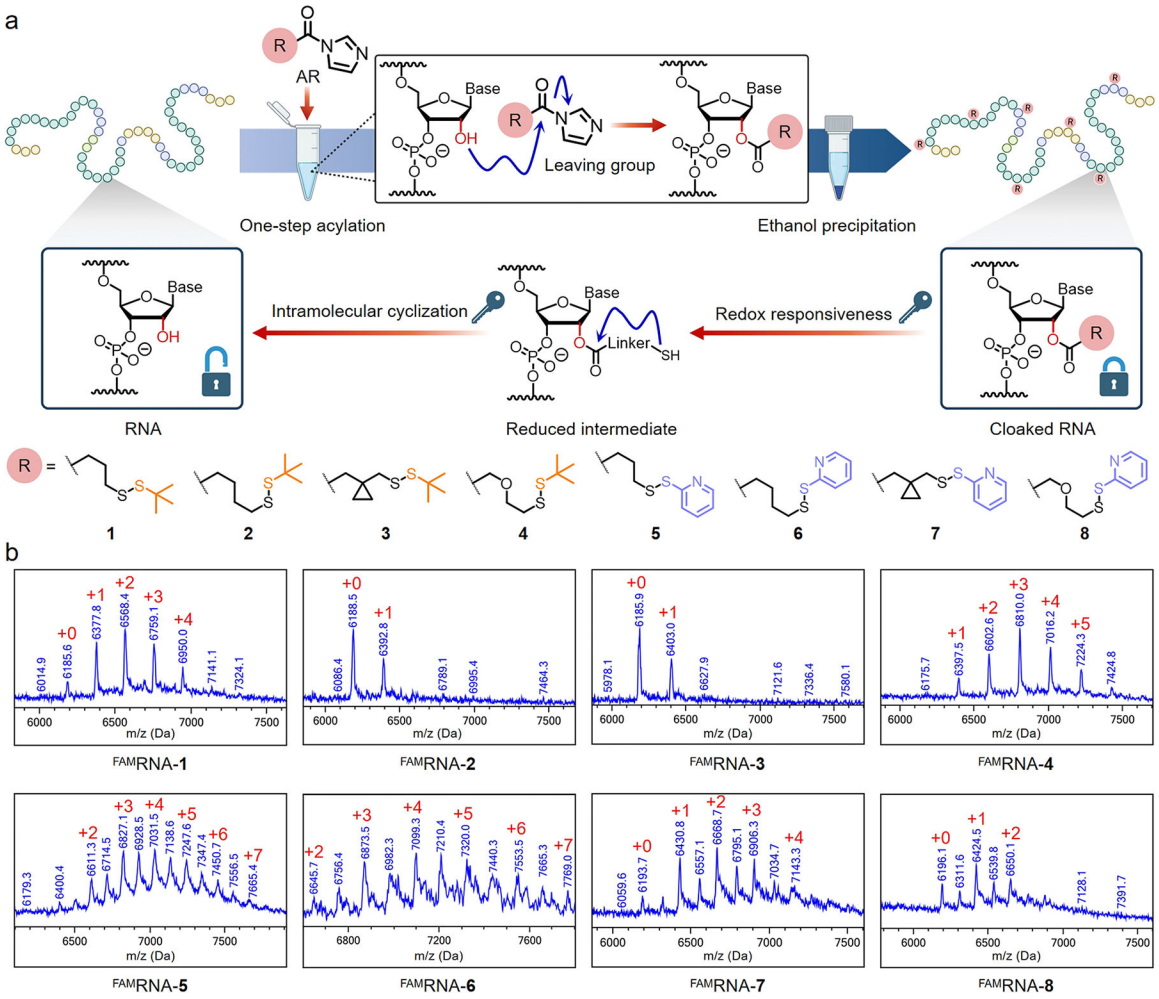

Figure 1.

a) Polyacylation of 2′-OH groups (cloaking) by acylating reagents (ARs) and purification by ethanol precipitation. Treatment with reducing stimuli removes acyl groups (uncloaking) and restores RNA structures and functions. b) MALDI-TOF mass spectra of cloaked ^{FAM}RNAs. The number of acyl adducts is displayed in red for each peak. The calculated mass of native ^{FAM}RNA is 6187.9. Note that the high-power laser used in the laser desorption possibly broke the disulfide bonds, as the masses of partially adducted RNAs reflect loss of the thiopyridyl group.

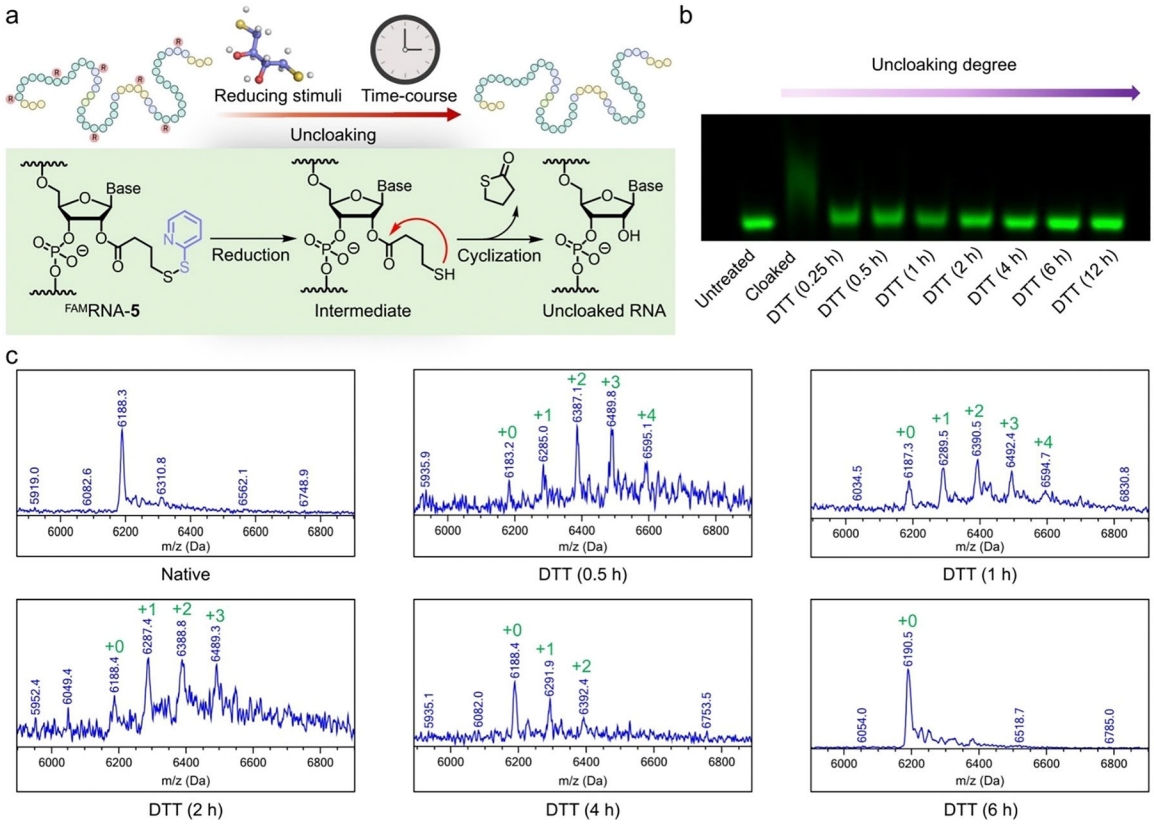

Figure 2.

a) Experimental workflow to evaluate the uncloaking kinetics of cloaked ^{FAM}RNA by reducing stimuli, taking ^{FAM}RNA-**5** for example. b) ^{FAM}RNA-**5** was treated with 10 mM DTT at 37°C and pH 7.4 for the indicated time points, analyzed by 20% denaturing PAGE. The full-size gel is shown in Figure S17. c) Time-course uncloaking of ^{FAM}RNA-**5** by incubation with 10 mM DTT (37°C, pH 7.4) indicates no detectable disulfides (loss of thiopyridyl groups) within 0.5 h and a gradual removal of reduced acyl groups. The calculated mass of native ^{FAM}RNA is 6187.9. The number of reduced acyl adducts is displayed in green for each corresponding peak in the MALDI-TOF spectra.

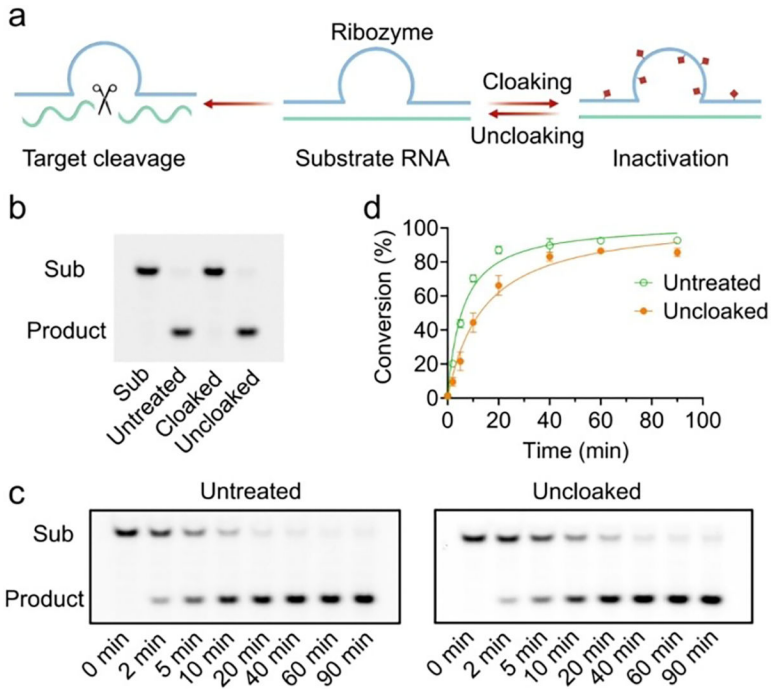

Figure 3.

a) Schematic of ribozyme-mediated cleavage of target substrate. Cloaking/uncloaking control the catalytic activity of ribozyme. b) Denaturing PAGE (15%) analysis of substrate cleavage after incubation with ribozyme for 1.5 h, the gel is shown from left to right: substrate RNA only, untreated ribozyme/substrate, **5** cloaked ribozyme/substrate, and uncloaked ribozyme/substrate (10 mM DTT for 6 h at 37°C, pH 7.4). c) Time course of cleavage of 100 nM untreated ribozyme against 250 nM substrate (left), and 100 nM uncloaked ribozyme against 250 nM substrate (right, 10 mM DTT for 6 h at 37°C, pH 7.4), analyzed by 15% denaturing PAGE and d) quantified using densitometry of gel bands, and conversion was calculated using the expression P/(S+P). Each data point for the set of untreated ribozyme/substrate and uncloaked ribozyme/substrate is represented as green circles and orange circles, respectively. Data represent mean±s.e.m., n=3 independent experiments. The full-size gels for Figure 3b,3c are shown in Figure S17.

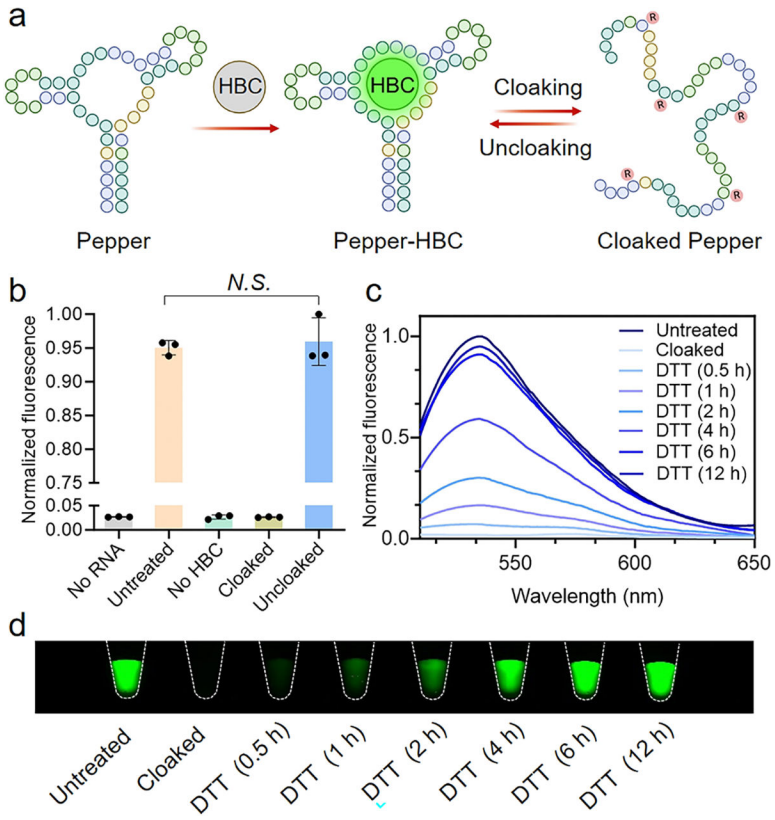

Figure 4.

a) Schematic illustration of the fluorescence emission of Pepper-HBC complex. Cloaking/uncloaking control RNA folding and HBC dye binding. b) Total fluorescence of untreated, cloaked, and uncloaked Pepper aptamers with HBC. Pepper aptamer cloaked with AR **5** (100 mM) in buffer, resulted in a loss of fluorescence, which was fully restored by incubation with 10 mM DTT for 6 h at 37°C, pH 7.4. c) Time-course recovery of fluorescence emission spectra of Pepper aptamer. Fluorescence was markedly reduced after cloaking (100 mM AR **5**), and was gradually restored by treatment with DTT at 37°C and pH 7.4 for the indicated time points. d) Fluorescence intensity of cloaked Pepper aptamers in relation to different uncloaking durations, visualized by Typhoon fluorescence imaging. Data represent mean±− s.e.m., n=3 independent experiments. Statistical significance was calculated with two-tailed unpaired Student's t-tests: *N.S.* indicates no significant difference.

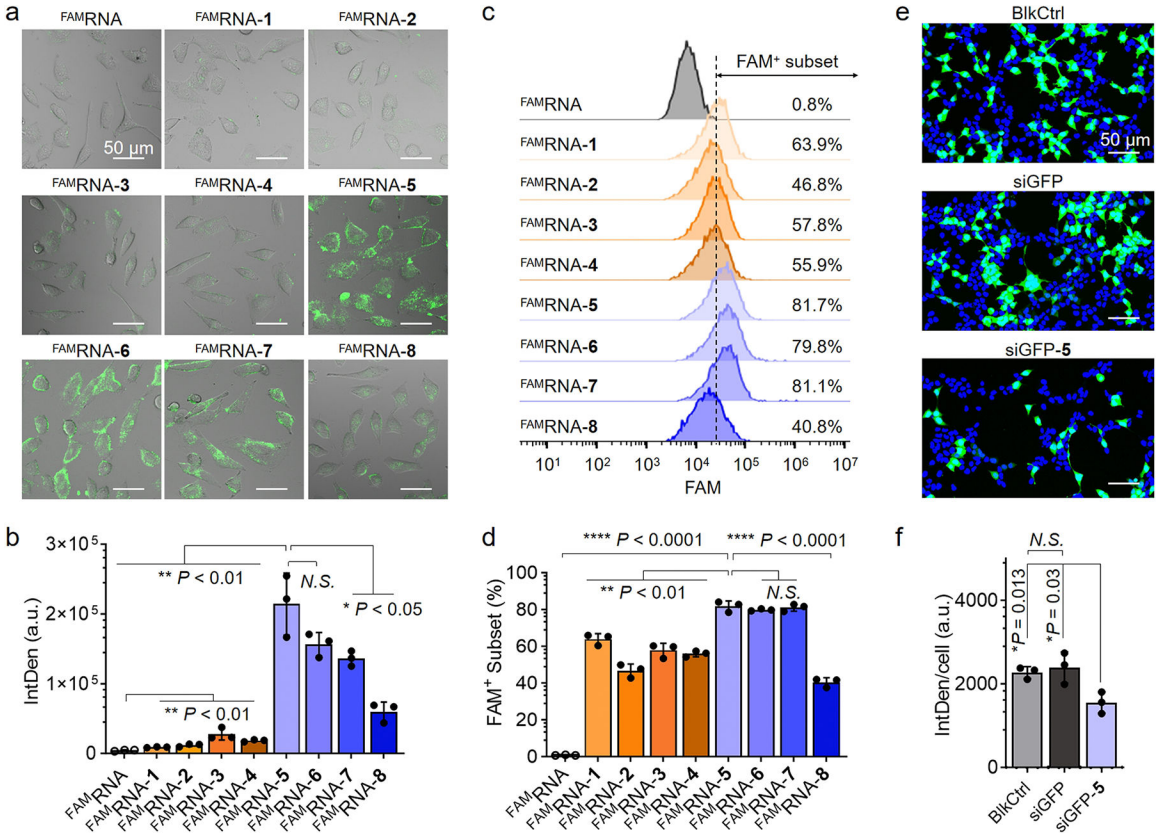

Figure 5.

a) Representative CLSM images of HeLa cells after 1-h incubation with 200 nM ^{FAM}RNA-ARs (green), scale bars=50 μm. b) The averaged integrated optical density (IntDen) of green fluorescence intensity in a) was quantitated by ImageJ software. c-d) Flow cytometry analysis of cellular uptake of ^{FAM}RNA-ARs (200 nM, 1-h incubation) in HeLa cells as determined by ^{FAM}RNA-positive subsets. e) Representative CLSM images of GFP-expressing HEK293T cells after 48-h incubation with 200 nM of siGFP or siGFP-**5**; nuclei were stained with Hoechst 33342 (blue), scale bars=50 μm. f) The average IntDen of green fluorescence per cell in e) was quantitated by ImageJ software. Data represent mean±s.e.m., n=3 independent experiments. Statistical significance was calculated with two-tailed unpaired Student's t-test: P values are indicated above the plots; *N.S.* indicates no significant difference.

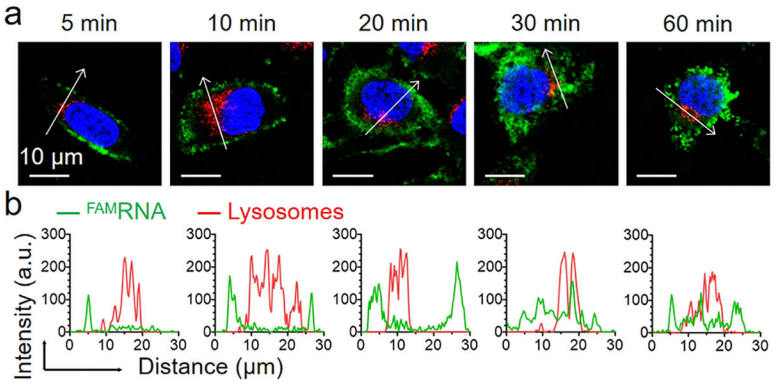

Figure 6.

a) Time-lapse imaging of the cellular uptake of green ^{FAM}RNA-**5** (200 nM) and its colocalization with lysosomes in HeLa cells; nuclei were stained with Hoechst 33342 (blue) and lysosomes were stained with LysoTracker Red DND-99 (red), scale bars=10 μm. b) The line scan analysis of fluorescence, along with the indicated white arrows, was performed by ImageJ software to determine the distribution of ^{FAM}RNA-**5** (green) and lysosomes (red).